Changes in membrane biophysical properties induced by sphingomyelinase depend on the sphingolipid *N*-acyl chain

Sandra N. Pinto,* Elad L. Laviad,[†] Johnny Stiban,[1,†] Samuel L. Kelly,[§] Alfred H. Merrill, Jr.,[§] Manuel Prieto,* Anthony H. Futerman,[†] and Liana C. Silva[2,**]

Centro de Química-Física Molecular and Institute of Nanoscience and Nanotechnology,* Instituto Superior Técnico, Universidade de Lisboa, 1049-001 Lisboa, Portugal; Department of Biological Chemistry,[†] Weizmann Institute of Science, Rehovot 76100, Israel; School of Biology and Petit Institute for Bioengineering and Bioscience,[§] Georgia Institute of Technology, Atlanta, GA 30332-0230; and iMed.UL,** Faculdade de Farmácia Universidade de Lisboa, 1649-003 Lisboa, Portugal

Abstract   Ceramide (Cer) is involved in the regulation of several cellular processes by mechanisms that depend on Cer-induced changes on membrane biophysical properties. Accumulating evidence shows that Cers with different *N*-acyl chain composition differentially impact cell physiology, which may in part be due to specific alterations in membrane biophysical properties. We now address how the sphingolipid (SL) *N*-acyl chain affects membrane properties in cultured human embryonic kidney cells by overexpressing different Cer synthases (CerSs). Our results show an increase in the order of cellular membranes in CerS2-transfected cells caused by the enrichment in very long acyl chain SLs. Formation of Cer upon treatment of cells with bacterial sphingomyelinase promoted sequential changes in the properties of the membranes: after an initial increase in the order of the fluid plasma membrane, reorganization into domains with gel-like properties whose characteristics are dependent on the acyl chain structure of the Cer was observed. Moreover, the extent of alterations of membrane properties correlates with the amount of Cer formed. These data reinforce the significance of Cer-induced changes on membrane biophysical properties as a likely molecular mechanism by which different acyl chain Cers exert their specific biological actions.**—Pinto, S. N., E. L. Laviad, J. Stiban, S. L. Kelly, A. H. Merrill, Jr., M. Prieto, A. H. Futerman, and L. C. Silva. Changes in membrane biophysical properties induced by sphingomyelinase depend on the sphingolipid *N*-acyl chain.** *J. Lipid Res.* **2014.** 55: **53–61.**

Supplementary key words   sphingolipids • acyl chain structure • ceramide • lipid domains • ceramide synthases • membrane remodeling

Sphingolipids (SLs) are vital components of biological membranes and are involved in a variety of biological processes ranging from cell proliferation to apoptosis [e.g., (1–3)]. Ceramide (Cer) is the hydrophobic backbone of all complex SLs and consists of a fatty acid of variable chain length linked by an amide bond to C2 of the long chain base, which is typically sphingosine or sphinganine (2). Elevation of Cer levels in response to stress stimuli involves predominantly sphingomyelin (SM) degradation (3). Under the influence of several agents (e.g., Fas ligand, TNF-α, nitric oxide), SM is hydrolyzed by sphingomyelinases (SMases) to generate Cer, driving the formation of Cer-enriched domains, also known as Cer platforms (4–9). The formation of these platforms has a strong impact on cell biology as the tightly packed Cer molecules induce the clustering of cell death receptors which initiate signaling cascades that ultimately lead to cell death (4). This evidence raised the hypothesis that the biophysical properties of Cer may directly modulate biological processes. In addition, it has been suggested that Cer-dependent cellular responses are specifically regulated by the acyl chain composition of SLs and Cer. Indeed, the existence of six distinct Cer synthases (CerSs) that specifically regulate the fatty acid composition of Cer (10) and display differential tissue distribution

(11, 12) suggests that different Cer species play distinct roles in cell physiology (10, 11). Thus, understanding how membrane biophysical properties are affected upon generation of Cer with specific acyl chains is crucial for understanding the correlation between the cellular roles of Cer and its biophysical properties.

To date, several biophysical studies [e.g., (13–19)] have focused on the effect of Cer on the properties of model membranes and have demonstrated that Cer increases the global order of the membrane and promotes lateral phase separation in a manner dependent on its acyl chain structure (19–21). However, no information is currently available on the effect of altering the Cer acyl chain length on the properties of cell membranes. In this study, we investigate the effect of generating Cer in human embryonic kidney (HEK) cells overexpressing different CerSs, i.e., having distinct SL acyl chain compositions. Using a combination of fluorescent probes that display different phase-related properties (22), we show that the biophysical properties of the plasma and intracellular membranes change with the SL acyl chain composition of the cells. Moreover, Cer formation promotes extensive membrane remodeling in a manner that correlates with the acyl chain composition of the Cer that is generated. These results support the hypothesis that Cer-induced changes on membrane biophysical properties might be responsible for Cer-mediated biological processes.

MATERIALS AND METHODS

Materials

1,2-Dioleoyl-*sn*-glycero-3-phosphoethanolamine-*N*-(lissamine rhodamine-B-sulfonyl) (Rho-DOPE) and *N*-{6-[(7-nitro-2,1,3-benzoxadiazol-4-yl)amino]hexanoyl}sphingosine-1-phosphocholine (C6-NBD-SM) were from Avanti Polar Lipids (Alabaster, AL). 1,2-Dipalmitoyl-*sn*-glycero-3-phosphoethanolamine-*N*-(7-nitro-2-1,3-benzoxa-diazol-4-yl) (NBD-DPPE), 1,6-diphenyl-1,3,5-hexatriene (TMA-DPH), and trans-parinaric acid (t-PnA) were from Molecular Probes (Leiden, The Netherlands). SMase isolated from *Bacillus cereus* was from Sigma (St. Louis, MO). Phosphate-buffered saline (PBS) (pH 7.4) and cell culture reagents were from Invitrogen (Breda, The Netherlands). Silica gel 60 TLC plates were from Merck (Darmstadt, Germany). All organic solvents were UVASOL grade from Merck.

Cell culture and transfection

HEK 293 cells were cultured in DMEM supplemented with 10% FBS, 100 IU/ml penicillin, and 100 μg/ml streptomycin in a 5% CO_2 incubator at 37°C. HEK 293 cells were transfected with human CerS genes using the calcium phosphate method (20 μg of plasmid per 10 cm culture plate) as described (23).

Metabolic assays

To quantify the conversion of SM into Cer, HEK cells were collected ($\sim 1 \times 10^6$ cells/ml) in PBS (with calcium and magnesium), incubated with C6-NBD-SM (2 μM) in the presence or absence of bacterial SMase (bSMase). The reaction was terminated by addition of $CHCl_3$/methanol (1:2 v/v) and lipids separated by TLC using $CHCl_3$/methanol/9.8 mM $CaCl_2$ (60:35:8 v/v/v) as the developing solvent. C6-NBD-SM and C6-NBD-Cer were used as standards. TLC plates were imaged using a Typhoon 9410 (Amersham

Biosciences) and bands were analyzed with Image Quant TL software (Amersham Biosciences).

Cytotoxicity assays

The in vitro cytotoxicity assay was evaluated as previously described (24). Briefly, HEK cells were plated at 1×10^4 cells/well in 96-well plates and cultured overnight. After this step, the cell medium was replaced with fresh medium containing 0.5 U/ml bSMase. The release of lactate dehydrogenase (LDH) into the medium was quantified by using a Cytotoxicity Detection Kit[PLUS] (LDH) according to the manufacturer's instructions (Roche). LDH release (percent cytotoxicity) was quantified by using the following equation: [Absorption at 492 nm (Abs_{492}) for experimental release − Abs_{492} for spontaneous release]/(Abs_{492} for maximum release − Abs_{492} for spontaneous release) × 100. The spontaneous release was the amount of LDH released from the cytoplasm of untreated cells, whereas the maximum amount of releasable LDH enzyme activity was determined by lysing the cells with Triton X-100.

Electrospray ionization-tandem mass spectrometry

HEK 293 cells were transfected with human CerS2 or human CerS5, and after 36 h were harvested by trypsinization, collected by centrifugation, washed twice with ice-cold PBS, and lyophilized. SL analyses by electrospray ionization-tandem mass spectrometry (MS/MS) were conducted using a PE-Sciex API 3000 triple quadrupole mass spectrometer and an ABI 4000 quadrupole-linear ion trap mass spectrometer (25). SL levels were normalized to pmol/mg of dry weight and data were plotted as a molar fraction of total SLs (26).

Fluorescence anisotropy and lifetime measurements

To follow alterations in membrane biophysical properties, fluorescence anisotropy and lifetimes of different probes were measured at different time points in the absence and presence of different concentrations of bSMase. All measurements were performed in 0.5 cm × 0.5 cm quartz cuvettes under magnetic stirring. Steady-state fluorescence measurements were performed with a FluoroLog spectrofluorometer from Horiba Jobin Yvon (Kyoto, Japan) using 320/405, 358/430, 465/536, 570/593 nm excitation (λ_{exc})/emission (λ_{em}) wavelengths for t-PnA, TMA-DPH, NBD-DPPE, and Rho-DOPE, respectively. The final probe concentration was 2 μM for t-PnA and TMA-DPH, 1.2 μM for NBD-DPPE, and 0.8 μM for Rho-DOPE in $\sim 1 \times 10^6$ cells/ml.

Fluorescence lifetime measurements were performed in a FluoroLog spectrofluorometer from Horiba Jobin Yvon and were obtained by the time-correlated single photon counting technique with fixed-wavelength "plug and play" interchangeable NanoLED pulsed laser diodes of 295 nm for t-PnA. The experimental decays were analyzed using TRFA software (Scientific Software Technologies Center, Minsk, Belarus). For a decay described by a sum of exponentials, where α_i is the normalized preexponential and τ_i is the lifetime of the decay component i, the mean fluorescence lifetime is given by the following (27):

$$\langle \tau \rangle = \sum_i \alpha_i \tau_i^2 \Big/ \sum_i \alpha_i \tau_i$$

All data were corrected for background (intrinsic cell fluorescence) by subtracting a blank (cells without probe) prepared and measured under exactly the same conditions as the samples (cells with probe).

Statistical analysis

A Student's *t*-test was used for statistical comparisons among groups and differences were considered statistically significant when $P < 0.05$ (*$P < 0.05$; **$P < 0.01$; ***$P < 0.001$).

Characterization of SL species in HEK cells

HEK cells are mainly enriched in long acyl chain (LC)-SLs (C16–C20) (11, 28, 29) (**Fig. 1**). To evaluate the impact of SL acyl chain composition on membrane biophysical properties, HEK cells were transfected with CerS2 in order to increase levels of very long acyl chain (VLC)-SLs (C22–C24) (Fig. 1) or with CerS5 to increase levels of C16-SLs (10, 11) (Fig. 1). Similar to previous results (11), transfection of HEK cells with CerS2 resulted in a significant increase in VLC-SLs (Fig. 1A, B) and a slight increase in unsaturated SLs (Fig. 1C), which was mainly due to elevation in levels of C24:1-SLs. In contrast, transfection with CerS5 caused an increase in C16-SLs (Fig. 1A), which was accompanied by a slight increase in saturated SLs (Fig. 1C) and a reduction in VLC-SLs (Fig. 1B). It should be emphasized that SM is the most abundant SL in cells, constituting ∼70% of total SLs. In addition, even in CerS2-transfected cells, C16-SM is the major SM species, constituting about 65, 60, and 70% of the total SM species in mock-, CerS2-, and CerS5-transfected cells, respectively (Fig. 1A). VLC-SMs comprise 19, 24, and 15% of total SM species in mock-, CerS2-, and CerS5-transfected cells, respectively.

Influence of SL acyl chain structure on membrane biophysical properties

The effects of changing the SL acyl chain composition on the biophysical properties of cell membranes were evaluated by fluorescence spectroscopy using multiple fluorescent probes. Each of these probes presented different phase-related properties and preferential partition into distinct phases (20, 22, 30, 31), allowing the identification and characterization of those phases. In addition, some of the probes were expected to localize predominantly in the outer leaflet of the plasma membrane (PM) (such as, NBD-DPPE, TMA-DPH, and Rho-DOPE), whereas others

were expected to distribute among all cellular membranes (t-PnA). This methodology allowed identification of the alterations undergone on the PM and in whole cells. It should be noted that the experimentally determined fluorescence anisotropy and lifetime are weighted averages of these parameters which reflect the partitioning of the probes between heterogeneous environments and not the order of a specific membrane. Therefore, the experimentally determined values depend on the biophysical properties of the membrane, the fraction of each phase, and the partition coefficient of the probe toward that phase.

NBD-DPPE is a saturated phospholipid with a NBD chromophore in the headgroup. The bulky headgroup prevents extensive flip-flop of the probe (32), and thus the probe should be localized mainly in the outer leaflet of the PM. In addition, NBD-DPPE has a preference to incorporate into ordered membrane regions (30, 33, 34). Therefore, even if only a small fraction of the lipids are organized in ordered phases, the anisotropy of NBD-DPPE will increase. The fluorescence anisotropy of NBD-DPPE (**Fig. 2A**) was higher in CerS2-transfected cells, showing that altering the SL metabolism toward the formation of VLC-SLs causes an increase in global order of the PM or in the fraction of ordered regions. Because the anisotropy of this PM probe (NBD-DPPE) changes compared with mock-transfected cells, this suggests that the PM lipid composition is probably altered in CerS2-transfected cells. From these results, it can be hypothesized that this likely derives from an enrichment of VLC-SLs at the PM of CerS2-transfected cells. No significant differences were observed in mock- and CerS5-transfected cells, although NBD-DPPE anisotropy was slightly higher in the latter (Fig. 2A).

The bulky headgroup of Rho-DOPE also prevents extensive flip-flop of this probe (32), which contributes to a preferential localization of Rho-DOPE in the outer leaflet of the PM. In addition, this probe has the peculiarity of presenting a strong overlap between the excitation and emission spectra, which contributes to a high probability
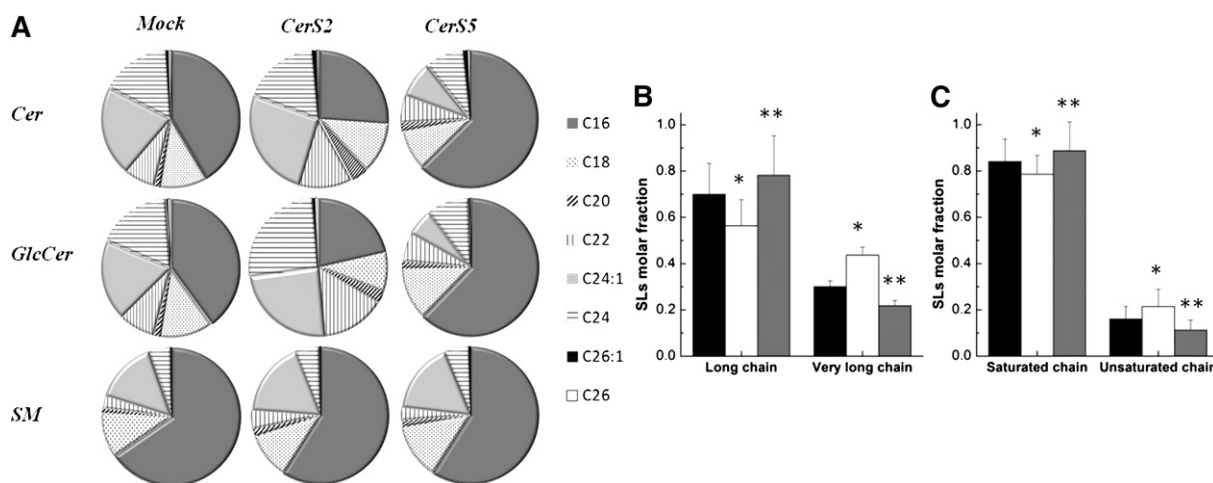
Fig. 1. The distribution of *N*-acyl chain SLs in HEK cells. A: ESI-MS/MS was used to determine the percent distribution of acyl chains in Cer, SM, and glucosylceramide in mock-, CerS2-, and CerS5-transfected HEK cells. B: Molar fraction of LC-SLs (C16–C20) and VLC-SLs (C22–C26). C: Molar fraction of saturated and unsaturated SL species. Data for mock-, CerS2-, and CerS5-transfected cells are shown in black, white, and gray, respectively. The values are the average (±SD) of n ≥ 3; *$P < 0.05$; **$P < 0.01$.
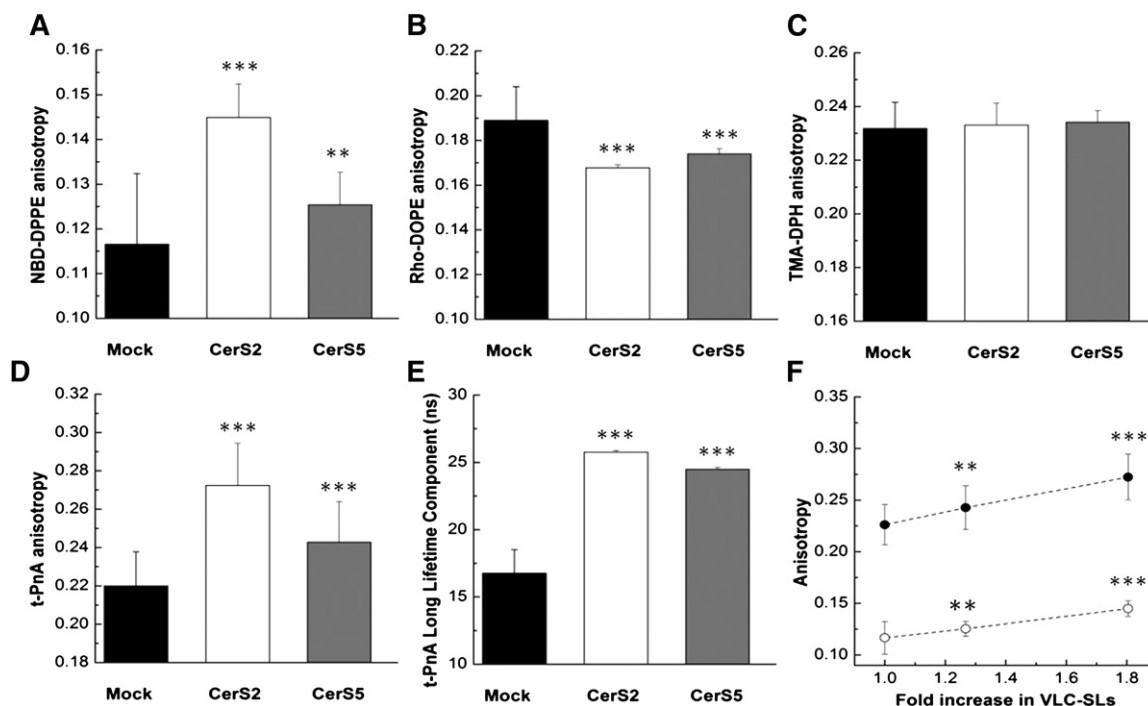
Fig. 2. Effect of SL acyl chain structure on the biophysical properties of HEK cells overexpressing different CerSs. Fluorescence anisotropy of NBD-DPPE (A), Rho-DOPE (B), TMA-DPH (C), t-PnA (D), and long lifetime component of t-PnA fluorescence intensity decay (E) in mock- (black), CerS2- (white), and CerS5-transfected (gray) HEK cells. F: Fluorescence anisotropy of t-PnA (●) and NBD-DPPE (○) represented as a function of the fold-increase in VLC-SLs. All experiments were performed at 37°C. The values are the average (±SD) of n ⩾ 3; **$P < 0.01$; ***$P < 0.001$.

of energy homotransfer (energy migration) (35). The efficiency of energy transfer will increase as the distance that separates the two chromophores decreases. The extent of energy migration is evaluated from the decrease in the fluorescence anisotropy of the probe. Figure 2B shows that Rho-DOPE fluorescence anisotropy was higher in mock-transfected HEK cells and lower in CerS2-transfected HEK cells, showing that the extent of energy migration was higher in CerS2-transfected cells. These results suggest enrichment in ordered membrane regions in CerS2- compared with mock- and CerS5-transfected cells. The reason for this resides in the fact that Rho-DOPE is excluded from ordered membrane regions (36). Therefore, an increase in the fraction of these regions will lead to a reduction in the surface area for probe distribution (i.e., of disordered membrane regions), implying concomitant increase in the local probe concentration, and thus a decrease in the distance between Rho molecules.

TMA-DPH is a probe that partitions equally between ordered and disordered phases. Accordingly, significant changes in its anisotropy are only expected if a significant fraction of the lipids are involved in the formation of ordered phases. Figure 2C shows that the anisotropy of TMA-DPH was essentially identical in mock-, CerS2-, and CerS5-transfected HEK cells, suggesting that alterations in the lipid composition of the PM of CerS2-transfected cells cause only a moderate increase in the fraction of ordered membrane regions.

t-PnA has the ability to flip-flop across the membrane and diffuses rapidly between membranes (37). Accordingly,

this probe will be localized not only in the PM but also in intracellular membranes. This probe displays an equal partition between ordered and disordered phases, and a strong partitioning into gel-like phases (13). Moreover, its quantum yield is enhanced in the gel phase, so the fluorescence intensity that arises from the probe located in the gel phase is enhanced. t-PnA fluorescence anisotropy (Fig. 2D) and the long lifetime component of the fluorescence intensity decay (Fig. 2E) were significantly higher in CerS2-transfected cells, suggesting that increasing levels of VLC-SLs leads to an increase in the order of cell membranes compared with cells that are enriched in LC species, i.e., mock- and CerS5-transfected cells. The slightly higher anisotropy and long lifetime component of the fluorescence intensity decay of t-PnA in CerS5-transfected cells, compared with HEK cells, is also suggestive of an increase in membrane order. The reason for this might be due to the global increase in saturated SLs species in these cells (Fig. 1C). It should be noted that the high anisotropy values and fluorescence lifetime measured with t-PnA reflect a higher global order and/or fraction of membrane ordered regions in cellular membranes, and not specifically in the PM, as mentioned above. Therefore, these results suggest that altering the SL metabolism toward the formation of VLC-SLs has an impact on the lipid composition and on cellular membrane properties. This is further supported by a progressive increase in the anisotropy of t-PnA and NBD-DPPE as the amount of VLC-SLs increases (Fig. 2F).

Effect of bSMase-generated Cer on membrane biophysical properties

To study the biophysical effect of generating Cer in the PM of cultured cells, bSMase was added to HEK cells and the kinetics of SM hydrolysis examined over time (**Fig. 3A**). Addition of bSMase to the cells resulted in a time-dependent conversion of NBD-SM until 80–90% of the substrate was hydrolyzed. The rate of SM hydrolysis increased with increasing concentrations of bSMase: for the highest bSMase concentration (0.5 U/ml), 80–90% of SM-to-Cer conversion was attained 5 min after addition of the enzyme, whereas longer times were required for lower bSMase concentrations. To evaluate whether cells were still viable after bSMase treatment, cell cytotoxicity was assayed (inset in Fig. 3A). Even for the highest bSMase concentration used, cell cytotoxicity was always below 5%, showing that under the experimental conditions employed in this study, and in the time range of the experiments, no massive cytotoxicity occurred.

The alterations in membrane biophysical properties upon addition of different concentrations of bSMase were monitored over time by t-PnA fluorescence anisotropy (Fig. 3B). In the absence of bSMase, the anisotropy of t-PnA was constant, demonstrating that no significant alterations occurred during the time of the experiment. In the presence of bSMase, an increase in t-PnA anisotropy was observed after a lag period. The lag time increased with decreasing concentrations of the enzyme. These results suggest that the formation of Cer drives an increase in the order of the membrane and that the changes in membrane properties correlate with the amount of Cer that is formed.

Effect of Cer acyl chain structure on membrane biophysical properties

To address the biophysical effect of generating different acyl chain length Cers, bSMase was externally added to mock-, CerS2-, and CerS5-transfected HEK cells. In these studies, we used the highest bSMase concentration in order to minimize the time required to generate Cer. Previous studies show that bSMase has essentially no substrate specificity, and is therefore able to hydrolyze LC- and VLC-SMs to a similar extent (38). In the present study, we evaluated the kinetics of SM hydrolysis in mock-, CerS2-, and CerS5-transfected cells (**Fig. 4A**). The results are similar, suggesting that bSMase similarly hydrolyzes the different SM species that are localized in the PM.

The alterations in membrane biophysical properties in response to bSMase-generated Cer were again monitored over time using multiple fluorescent probes (Fig. 4B). Upon addition of bSMase to the cells, there was an immediate increase in NBD-DPPE (Fig. 4B, C) and TMA-DPH (Fig. 4D) fluorescence anisotropy showing that SM hydrolysis promotes a rapid increase in the order of the PM. After 20 min, the fluorescence anisotropy of the probes reached their maximum values and no further alterations in PM properties were observed. This is further confirmed by the rapid decrease of Rho-DOPE fluorescence anisotropy in response to Cer formation (Fig. 4B, E). The time-course of membrane alterations, as detected by these probes, was similar in all cells. However, significant differences in the global order of the PM upon Cer formation were observed between mock-, CerS2-, and CerS5-transfected cells suggesting that the PM lipid composition of these cells differs, most likely due to the formation of Cers with specific acyl chains, which would change the membrane properties to different extents. If this is the case, the results suggest that formation of VLC- Cers (CerS2-transfected cells) have a stronger impact on the order of the PM because greater alterations in the fluorescence anisotropy of NBD-DPPE and Rho-DOPE are observed.

The time-course of variation of t-PnA fluorescence anisotropy (Fig. 4B, F), mean fluorescence lifetime (**Fig. 5A–C**), and long lifetime component (Fig. 5D) in response to SM hydrolysis was distinct from the other probes (Fig. 4B): a smaller increase in t-PnA photophysical parameters was observed up to 15–20 min of hydrolysis, after which an increase in the fluorescence anisotropy and a sharp increase
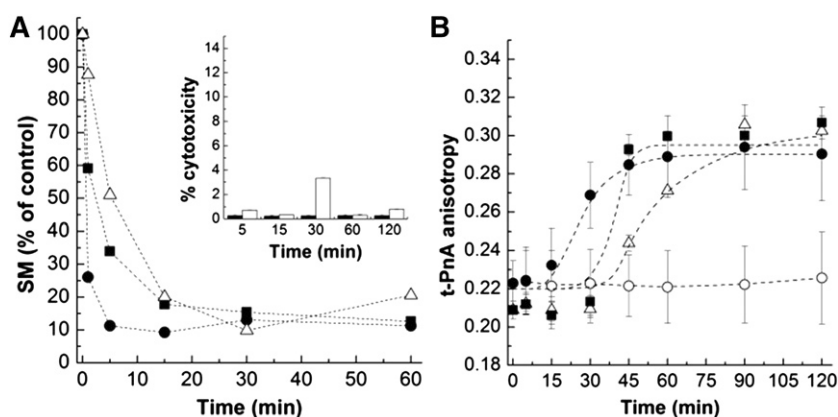
Fig. 3. Impact of Cer generated from bSMase on HEK cells. SM hydrolysis (A) and the fluorescence anisotropy of t-PnA (B) were followed over time in HEK cells upon treatment with 0.05 U/ml (△), 0.1 U/ml (■), and 0.5 U/ml (●) of bSMase. In (B) data for untreated cells (○) are also shown. The inset in (A) represents the results from a cell viability test. Cell cytotoxicity was determined by LDH assay in HEK cells in the absence (black columns) and presence (white columns) of bSMase. The values are the average (±SD) of n ≥ 3; all measurements were performed at 37°C.
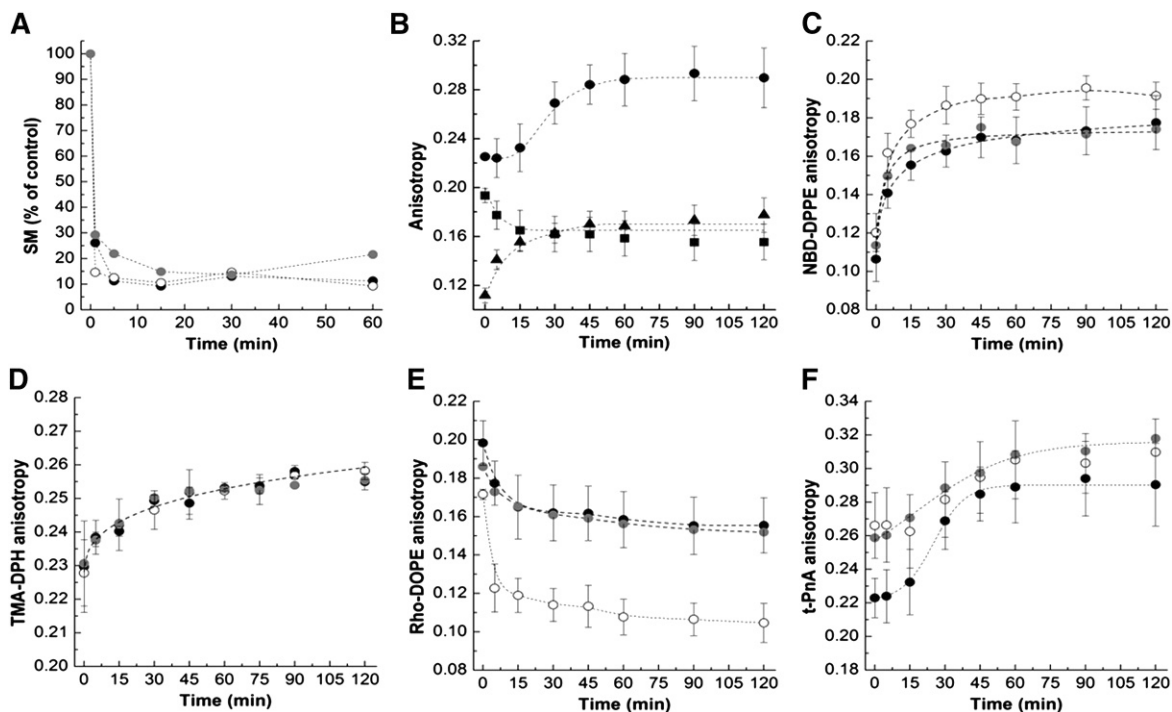
Fig. 4. Impact of bSMase-generated Cer in HEK cells overexpressing CerS2 or CerS5. A: SM hydrolysis in mock- (black circles),CerS2 (open circles)-, and CerS5-transfected (gray circles) HEK cells upon treatment with 0.5 U/ml of bSMase. B: Fluorescence anisotropy of t-PnA (●), Rho-DOPE (■), and NBD-DPPE (▲) was measured in mock-transfected cells to evaluate the time-dependent alterations undergone on the membrane upon treatment with 0.5 U/ml of bSMase. The fluorescence anisotropy of NBD-DPPE (C), TMA-DPH (D), Rho-DOPE (E), and t-PnA (F) was measured over time in cells treated with 0.5 U/ml of bSMase. The symbols are the same as in (A). The values are the average (±SD) of n ≥ 3; all measurements were performed at 37°C.

in the t-PnA long lifetime component of the fluorescence intensity decay and mean fluorescence lifetime were observed. The t-PnA long lifetime component is very long suggesting that gel-like domains are formed (13, 14, 22). This probe has a very high partition into gel domains and displays strong alterations in its photophysical parameters, therefore being extremely sensitive to the presence of gel domains. This can be appreciated by the increase in fluorescence anisotropy (Fig. 4F) and mean fluorescence lifetime (Fig. 5A–C) upon SM hydrolysis, but is particularly demonstrated by changes in the long lifetime component (Fig. 5D) of the fluorescence

intensity decay of t-PnA, which significantly increases when the gel phase is formed (14). This is because the higher lipid packing of the gel phase (higher rigidity) decreases the nonradiative pathway of the probe in the excited state, so a significant increase in the lifetime is observed for this forbidden transition [reviewed in (39)]. Therefore, the results suggest that the packing of the Cer-enriched phase in CerS5-transfected cells is higher compared with mock- and CerS2-transfected cells (Fig. 4F). This is likely to be related to the known packing properties of gel domains formed by C16:0-Cer (13, 14, 19, 22).
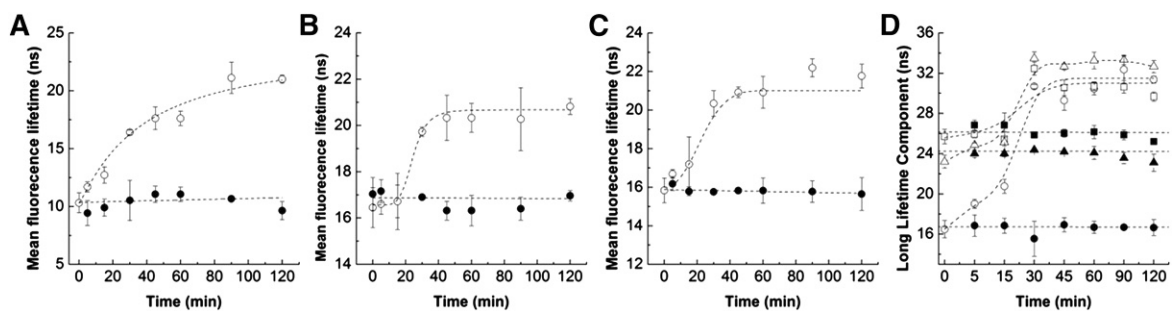
Fig. 5. Cer generation results in the formation of gel-like domains. Mean fluorescence lifetime of t-PnA in mock- (A), CerS2- (B), and CerS5-transfected (C) HEK cells in the absence (●) and presence (○) of 0.5 U/ml of bSMase. D: Long lifetime component of t-PnA fluorescence intensity decay was measured in the absence (closed symbols) and in the presence (open symbols) of 0.5 U/ml of bSMase in mock- (circles), CerS2- (squares), and CerS5-transfected (triangles) cells. The values are the average (±SD) of n ≥ 3; all measurements were performed at 37°C.

DISCUSSION

Influence of SL acyl chain structure on biophysical properties of plasma and intracellular membranes

We recently reported the effect of changing the acyl chain structure of SLs on the biophysical properties of microsomal lipid extracts from a WT and a CerS2-null mouse (26). In the present study, we have extended this approach to live cells. In order to induce an alteration in the acyl chain structure of the SLs, we transfected HEK cells with two different CerS genes: CerS2 and CerS5. Transfection with CerS2 promoted a significant increase in all VLC-SL species whereas, transfection with CerS5 increased levels of C16-SLs (10, 11). Although changes in SL acyl chain structure were not as marked as those observed in lipid extracts from a CerS2-null mouse (26), and C16-SLs were still the major components in the cells, significant differences in membrane biophysical properties were detected.

Not surprisingly, the anisotropy of the PM probes in HEK cells displayed intermediate values between disordered and ordered phases (14, 31), which reflects the complexity of lipid organization in membrane environments with distinct packing properties. The experimental anisotropy is the sum of the anisotropies of the probe in each phase weighted by the molar fraction of that phase. Accordingly, in cells, the experimental values correspond to an ensemble average of all anisotropies in the distinct lipid phases.

The distribution of SLs with distinct acyl chains in cellular membranes is currently unresolved. Most of the techniques used to identify and quantify lipid species, such as mass spectrometry, depend on the extraction of the lipids from cells and/or tissues and, thus, information regarding cellular localization is lost. Therefore, in the present study, we were unable to determine the localization of specific SLs, and their impact on a specific membrane can only be inferred from the variation of the photophysical properties of the probes located in the PM or in all cellular membranes. Our results show that membrane properties of CerS2-transfected cells differ from mock- and CerS5-transfected cells. This suggests an alteration in the lipid composition of these cells, which is possibly a consequence of enrichment in VLC-SLs. Because both the PM probes and t-PnA report alterations on membrane properties, our results further suggest that this change might occur both at the level of the PM and of intracellular membranes, which might be a consequence of alteration of the SL composition in different cellular membranes. Considering this hypothesis, the enrichment in VLC-SLs in CerS2-transfected cells might contribute to the formation of membrane regions enriched in these VLC-lipids that tend to segregate from other lipid components as a consequence of the strong mismatch between their chain structures, and therefore cause an increase in the fraction of ordered membrane regions. In addition, VLC-SLs have higher melting temperatures compared with LC-SLs [e.g., (40)], which contributes to a decrease in their miscibility with the other lipid components and consequent formation of more ordered membrane regions enriched in these high melting temperature SLs. The strong asymmetry of VLC-SLs might also affect the packing and the distribution of the bulk lipids in the bilayer by promoting the formation of interdigitated phases (19, 20, 40–42).

The results obtained in this study further suggest that the fraction of ordered PM regions only increases to a moderate extent in CerS2-transfected cells compared with mock- and CerS5-transfected cells. Based on what is known about the partitioning behavior of the probes used in the present study, it is possible to estimate the fraction of ordered regions formed at the PM. Considering the limiting situation of a model membrane containing only two phases, a gel and a fluid phase, where the anisotropy values of TMA-DPH in the pure gel and fluid phases are ∼0.28 and ∼0.205, respectively (20), an increase of at least 30% of the gel phase would be required to cause an increase in the anisotropy of ∼0.02. Note that this is an extreme example between a gel and fluid phase considering only the existence of two phases. Cellular membranes are much more complex and several different types of lipid phases with differences in their packing properties exist. Therefore, changes in the anisotropy of this probe would only be noticeable if the changes in the acyl chains of SL led to an increase of >50% of ordered membrane regions. It is also important to note that even though CerS2-transfected cells have higher proportions of VLC-SLs, LC-SLs nevertheless comprise the major amount of lipids in these cells and, in addition, it is not known if VLC-SLs are mainly localized in the PM or equally distributed in the cellular membranes. In view of that, it would not be expected that such ordered regions occupy an extensive area of the membrane.

Cer-induced membrane remodeling

A role has been proposed for Cer-induced alterations on membrane properties as the mechanism underlying the biological actions of Cer (43–45). However, two of the most intriguing questions regarding the mechanism by which ceramide activates cellular processes are: *i*) how does Cer change the properties of cell membranes; and *ii*) what is the underlying mechanism for the apparent specificity of Cer acyl chain structure in the regulation of specific functions? Linking membrane biophysics to cellular processes, it can be hypothesized that each Cer induces different changes in membrane properties that can be differentially sensed by its targets. Taking this hypothesis as a starting point, we evaluated the effect of increasing the PM levels of Cers in cells transfected with different CerSs, and thus that form Cers with distinct *N*-acyl chain structures.

Our results suggest a correlation between the level of Cer that is generated upon SM hydrolysis and Cer effects on membrane biophysical properties. To our knowledge, this is the first study showing a correlation between Cer formation in the PM and concomitant membrane biophysical changes in cells. Cleary, the changes observed on membrane properties do not depend exclusively on the formation of Cer, but also on its interplay with other lipids. It is important to stress that the interplay between Cer, SM, and cholesterol is important to the biophysical changes

driven by these lipids. Studies in model membranes demonstrated that Cer-gel domain formation is enhanced by the presence of SM (14, 22, 46). In contrast, large amounts of cholesterol are able to increase the solubility of Cer in the liquid-ordered phase (31, 47, 48). Accordingly, the effects promoted by Cer on the properties of cell membranes could be even stronger if SM was not hydrolyzed. Nevertheless, significant and immediate alterations on the PM properties (as monitored by all the PM probes used) were observed upon treating the cells with bSMase, suggesting that Cer drives massive changes on PM order. Note that a fast and substantial hydrolysis of SM was observed, which can account for the observed membrane biophysical changes. After 20–30 min of hydrolysis, no further alterations in the ordering state of the PM were detected, suggesting that membrane remodeling reaches equilibrium. This equilibrium state occurred in parallel with a sharp increase in the anisotropy and lifetime of t-PnA. It is noteworthy that the lifetime component now becomes very long and above the typical value obtained in a Cer-enriched highly ordered gel phase in model membranes (13, 14, 19), suggesting that this phase is probably being formed in the membrane.

The difference in the time-course of variation of the photophysical parameters of t-PnA and the PM probes suggests that two types of changes occur in the membranes: there is an initial increase in PM-ordered regions, followed by a reorganization of Cer into domains with gel-like properties. Considering that bSMase might act preferentially at the liquid-ordered/liquid-disordered interface (47, 49), the initial increase in the order of the PM would be consistent with the formation of Cer in regions enriched in cholesterol. The presence of cholesterol would contribute to an increase in the miscibility of Cer in the membrane (31, 48). Cer would then progressively organize into domains with gel-like properties. The packing of these domains is different in mock-, CerS2-, and CerS5-transfected cells, suggesting that their lipid composition is distinct, probably a consequence of the formation of Cers with different acyl chain structures. Interestingly, the gel-like domains formed in CerS5-transfected cells seem to be more tightly packed compared with those formed in mock- and CerS2-transfected cells. This might be due to an enrichment of LC-Cers in CerS5-transfected cells, which have been shown to form more tightly packed gel-domains compared with VLC-Cers (19, 20). The strong asymmetry of VLC-Cers promotes the formation of interdigitated gel phases which are typically less packed than a noninterdigitated gel phase (19, 20).

The results obtained with the PM probes NBD-DPPE and Rho-DOPE also suggest that different Cers are formed at the PM. As mentioned above, C16-SM is the major SM species, and is therefore likely one of the principal constituents of the PM. If the PM of HEK cells contained only C16-SL, treatment of the cells with bSMase would result in the formation of C16-Cer in all of the cells, independently of the CerS used for transfection. Under these conditions, it would be expected that similar changes in the PM biophysical properties of the CerS-transfected cells treated with bSMase would be observed. However, significant differences were observed, which can be explained by the formation of different acyl chain Cers in the PM. Accordingly, these results suggest that alterations in SL metabolism by transfecting cells with different CerSs leads to a change in the lipid composition of the PM, most likely due to the changes introduced in the acyl chain structure of the SL formed.

CONCLUSIONS

The results obtained in this study are the first to show the effect of changing the acyl chain composition of SLs on the biophysical properties of cell membranes in live cells. Moreover, this is also the first study identifying the alterations on membrane biophysical properties upon Cer formation in the PM. Several studies have suggested that in response to stress stimuli, Cer levels would increase in the PM promoting the formation of Cer platforms that are responsible for the activation of cellular processes due to the alterations in the biophysical properties of the membrane. However, no studies have provided information about the biophysical characteristics of Cer platforms. In the present study, we have shown that Cer promotes sequential changes in the properties of the membranes that seem to correlate with the extent of Cer formation in the PM. Furthermore, we have also shown that alteration of SL metabolism by expression of different CerSs drives distinct changes in the biophysical properties of membranes, suggesting a correlation between membrane properties and the acyl chain structure of the Cer that is formed. These observations reinforce the influence of membrane biophysical properties on the mechanism by which Cer exerts its biological actions, and particularly how distinct Cers might activate different processes by promoting different alterations in membrane properties.⬛⬛

REFERENCES

1. Lahiri, S., and A. H. Futerman. 2007. The metabolism and function of sphingolipids and glycosphingolipids. *Cell. Mol. Life Sci.* **64:** 2270–2284.
2. Ponnusamy, S., M. Meyers-Needham, C. E. Senkal, S. A. Saddoughi, D. Sentelle, S. P. Selvam, A. Salas, and B. Ogretmen. 2010. Sphingolipids and cancer: ceramide and sphingosine-1-phosphate in the regulation of cell death and drug resistance. *Future Oncol.* **6:** 1603–1624.
3. Huwiler, A., and J. Pfeilschifter. 2006. Altering the sphingosine-1-phosphate/ceramide balance: a promising approach for tumor therapy. *Curr. Pharm. Des.* **12:** 4625–4635.
4. Grassmé, H., V. Jendrossek, J. Bock, A. Riehle, and E. Gulbins. 2002. Ceramide-rich membrane rafts mediate CD40 clustering. *J. Immunol.* **168:** 298–307.
5. Grassmé, H., A. Riehle, B. Wilker, and E. Gulbins. 2005. Rhinoviruses infect human epithelial cells via ceramide-enriched membrane platforms. *J. Biol. Chem.* **280:** 26256–26262.
6. Schenck, M., A. Carpinteiro, H. Grassmé, F. Lang, and E. Gulbins. 2007. Ceramide: physiological and pathophysiological aspects. *Arch. Biochem. Biophys.* **462:** 171–175.
7. Stancevic, B., and R. Kolesnick. 2010. Ceramide-rich platforms in transmembrane signaling. *FEBS Lett.* **584:** 1728–1740.
8. Grassmé, H., V. Jendrossek, A. Riehle, G. von Kürthy, J. Berger, H. Schwarz, M. Weller, R. Kolesnick, and E. Gulbins. 2003. Host

defense against Pseudomonas aeruginosa requires ceramide-rich membrane rafts. *Nat. Med.* **9:** 322–330.

9. Rotolo, J. A., J. Zhang, M. Donepudi, H. Lee, Z. Fuks, and R. Kolesnick. 2005. Caspase-dependent and -independent activation of acid sphingomyelinase signaling. *J. Biol. Chem.* **280:** 26425–26434.

10. Pewzner-Jung, Y., S. Ben-Dor, and A. H. Futerman. 2006. When do Lasses (longevity assurance genes) become CerS (ceramide synthases)?: Insights into the regulation of ceramide synthesis. *J. Biol. Chem.* **281:** 25001–25005.

11. Laviad, E. L., L. Albee, I. Pankova-Kholmyansky, S. Epstein, H. Park, A. H. Merrill, and A. H. Futerman. 2008. Characterization of ceramide synthase 2: tissue distribution, substrate specificity, and inhibition by sphingosine 1-phosphate. *J. Biol. Chem.* **283:** 5677–5684.

12. Levy, M., and A. H. Futerman. 2010. Mammalian ceramide synthases. *IUBMB Life.* **62:** 347–356.

13. Silva, L., R. F. de Almeida, A. Fedorov, A. P. Matos, and M. Prieto. 2006. Ceramide-platform formation and -induced biophysical changes in a fluid phospholipid membrane. *Mol. Membr. Biol.* **23:** 137–148.

14. Silva, L. C., R. F. de Almeida, B. M. Castro, A. Fedorov, and M. Prieto. 2007. Ceramide-domain formation and collapse in lipid rafts: membrane reorganization by an apoptotic lipid. *Biophys. J.* **92:** 502–516.

15. Veiga, M. P., J. L. Arrondo, F. M. Goñi, and A. Alonso. 1999. Ceramides in phospholipid membranes: effects on bilayer stability and transition to nonlamellar phases. *Biophys. J.* **76:** 342–350.

16. Contreras, F-X., G. Basañez, A. Alonso, A. Herrmann, and F. M. Goñi. 2005. Asymmetric addition of ceramides but not dihydroceramides promotes transbilayer (flip-flop) lipid motion in membranes. *Biophys. J.* **88:** 348–359.

17. Sot, J., F. J. Aranda, M-I. Collado, F. M. Goñi, and A. Alonso. 2005. Different effects of long- and short-chain ceramides on the gel-fluid and lamellar-hexagonal transitions of phospholipids: a calorimetric, NMR, and x-ray diffraction study. *Biophys. J.* **88:** 3368–3380.

18. Chiantia, S., N. Kahya, J. Ries, and P. Schwille. 2006. Effects of ceramide on liquid-ordered domains investigated by simultaneous AFM and FCS. *Biophys. J.* **90:** 4500–4508.

19. Pinto, S. N., L. C. Silva, A. H. Futerman, and M. Prieto. 2011. Effect of ceramide structure on membrane biophysical properties: the role of acyl chain length and unsaturation. *Biochim. Biophys. Acta.* **1808:** 2753–2760.

20. Pinto, S. N., L. C. Silva, R. F. M. de Almeida, and M. Prieto. 2008. Membrane domain formation, interdigitation, and morphological alterations induced by the very long chain asymmetric C24:1 ceramide. *Biophys. J.* **95:** 2867–2879.

21. Carrer, D. C., E. Kummer, G. Chwastek, S. Chiantia, and P. Schwille. 2009. Asymmetry determines the effects of natural ceramides on model membranes. *Soft Matter.* **5:** 3279–3286.

22. Castro, B. M., R. F. M. de Almeida, L. C. Silva, A. Fedorov, and M. Prieto. 2007. Formation of ceramide/sphingomyelin gel domains in the presence of an unsaturated phospholipid: a quantitative multiprobe approach. *Biophys. J.* **93:** 1639–1650.

23. Kingston, R. E., C. A. Chen, and H. Okayama. 2001. Calcium phosphate transfection. *Curr. Protoc. Immunol.* **Chapter 10:** Unit 10.13.

24. Kodama, T., M. Rokuda, K-S. Park, V. V. Cantarelli, S. Matsuda, T. Iida, and T. Honda. 2007. Identification and characterization of VopT, a novel ADP-ribosyltransferase effector protein secreted via the Vibrio parahaemolyticus type III secretion system 2. *Cell. Microbiol.* **9:** 2598–2609.

25. Merrill, A. H., M. C. Sullards, J. C. Allegood, S. Kelly, and E. Wang. 2005. Sphingolipidomics: high-throughput, structure-specific, and quantitative analysis of sphingolipids by liquid chromatography tandem mass spectrometry. *Methods.* **36:** 207–224.

26. Silva, L. C., O. Ben David, Y. Pewzner-Jung, E. L. Laviad, J. Stiban, S. Bandyopadhyay, A. H. Merrill, M. Prieto, and A. H. Futerman. 2012. Ablation of ceramide synthase 2 strongly affects biophysical properties of membranes. *J. Lipid Res.* **53:** 430–436.

27. Lakowicz, J. R. 2006. Principles of Fluorescence Spectroscopy. 3rd edition. Springer, New York.

28. Venkataraman, K., C. Riebeling, J. Bodennec, H. Riezman, J. C. Allegood, M. C. Sullards, A. H. Merrill, and A. H. Futerman. 2002. Upstream of growth and differentiation factor 1 (uog1), a mammalian homolog of the yeast longevity assurance gene 1 (LAG1), regulates N-stearoyl-sphinganine (C18-(dihydro)ceramide) synthesis in a fumonisin B1-independent manner in mammalian cells. *J. Biol. Chem.* **277:** 35642–35649.

29. Lahiri, S., H. Park, E. L. Laviad, X. Lu, R. Bittman, and A. H. Futerman. 2009. Ceramide synthesis is modulated by the sphingosine analog FTY720 via a mixture of uncompetitive and noncompetitive inhibition in an Acyl-CoA chain length-dependent manner. *J. Biol. Chem.* **284:** 16090–16098.

30. de Almeida, R. F., L. M. Loura, A. Fedorov, and M. Prieto. 2005. Lipid rafts have different sizes depending on membrane composition: a time-resolved fluorescence resonance energy transfer study. *J. Mol. Biol.* **346:** 1109–1120.

31. Castro, B. M., L. C. Silva, A. Fedorov, R. F. M. de Almeida, and M. Prieto. 2009. Cholesterol-rich fluid membranes solubilize ceramide domains: implications for the structure and dynamics of mammalian intracellular and plasma membranes. *J. Biol. Chem.* **284:** 22978–22987.

32. Hope, M. J., T. E. Redelmeier, K. F. Wong, W. Rodrigueza, and P. R. Cullis. 1989. Phospholipid asymmetry in large unilamellar vesicles induced by transmembrane pH gradients. *Biochemistry.* **28:** 4181–4187.

33. Dietrich, C., L. A. Bagatolli, Z. N. Volovyk, N. L. Thompson, M. Levi, K. Jacobson, and E. Gratton. 2001. Lipid rafts reconstituted in model membranes. *Biophys. J.* **80:** 1417–1428.

34. Crane, J. M., and L. K. Tamm. 2004. Role of cholesterol in the formation and nature of lipid rafts in planar and spherical model membranes. *Biophys. J.* **86:** 2965–2979.

35. de Almeida, R. F., J. Borst, A. Fedorov, M. Prieto, and A. J. Visser. 2007. Complexity of lipid domains and rafts in giant unilamellar vesicles revealed by combining imaging and microscopic and macroscopic time-resolved fluorescence. *Biophys. J.* **93:** 539–553.

36. de Almeida, R. F., L. M. Loura, and M. Prieto. 2009. Membrane lipid domains and rafts: current applications of fluorescence lifetime spectroscopy and imaging. *Chem. Phys. Lipids.* **157:** 61–77.

37. Schroeder, F. 1980. Fluorescence probes as monitors of surface membrane fluidity gradients in murine fibroblasts. *Eur. J. Biochem.* **112:** 293–307.

38. Canals, D., R. W. Jenkins, P. Roddy, M. J. Hernandez-Corbacho, L. M. Obeid, and Y. A. Hannun. 2010. Differential effects of ceramide and sphingosine-1-phosphate on ERM phosphorylation: probing sphingolipid signaling at the outer plasma membrane. *J. Biol. Chem.* **285:** 32476–32485.

39. Berezin, M. Y., and S. Achilefu. 2010. Fluorescence lifetime measurements and biological imaging. *Chem. Rev.* **110:** 2641–2684.

40. Li, X. M., J. M. Smaby, M. M. Momsen, H. L. Brockman, and R. E. Brown. 2000. Sphingomyelin interfacial behavior: the impact of changing acyl chain composition. *Biophys. J.* **78:** 1921–1931.

41. Maulik, P. R., D. Atkinson, and G. G. Shipley. 1986. X-ray scattering of vesicles of N-acyl sphingomyelins. Determination of bilayer thickness. *Biophys. J.* **50:** 1071–1077.

42. Maulik, P. R., and G. G. Shipley. 1995. X-ray diffraction and calorimetric study of N-lignoceryl sphingomyelin membranes. *Biophys. J.* **69:** 1909–1916.

43. Henry, B., C. Möller, M-T. Dimanche-Boitrel, E. Gulbins, and K. A. Becker. 2013. Targeting the ceramide system in cancer. *Cancer Lett.* **332:** 286–294.

44. Goñi, F. M., and A. Alonso. 2009. Effects of ceramide and other simple sphingolipids on membrane lateral structure. *Biochim. Biophys. Acta.* **1788:** 169–177.

45. Zhang, Y., X. Li, K. A. Becker, and E. Gulbins. 2009. Ceramide-enriched membrane domains–structure and function. *Biochim. Biophys. Acta.* **1788:** 178–183.

46. Busto, J. V., M. L. Fanani, L. De Tullio, J. Sot, B. Maggio, F. M. Goñi, and A. Alonso. 2009. Coexistence of immiscible mixtures of palmitoylsphingomyelin and palmitoylceramide in monolayers and bilayers. *Biophys. J.* **97:** 2717–2726.

47. Silva, L. C., A. H. Futerman, and M. Prieto. 2009. Lipid raft composition modulates sphingomyelinase activity and ceramide-induced membrane physical alterations. *Biophys. J.* **96:** 3210–3222.

48. Pinto, S. N., F. Fernandes, A. H. Futerman, L. C. Silva, and M. Prieto. 2013. A combined fluorescence spectroscopy, confocal and 2-photon microscopy approach to re-evaluate the properties of sphingolipid domains. *Biochim. Biophys. Acta.* **1828:** 2099–2110.

49. Fanani, M. L., S. Hartel, B. Maggio, L. De Tullio, J. Jara, F. Olmos, and R. G. Oliveira. 2010. The action of sphingomyelinase in lipid monolayers as revealed by microscopic image analysis. *Biochim. Biophys. Acta.* **1798:** 1309–1323.